Engineering design of a cardiac myocyte

**W. J. Adams · T. Pong · N. A. Geisse · S. P. Sheehy ·
B. Diop-Frimpong · K. K. Parker**

Abstract   We describe a design algorithm to build a cardiac myocyte with specific spatial dimensions and physiological function. Using a computational model of a cardiac muscle cell, we modeled calcium (Ca^{2+}) wave dynamics in a cardiac myocyte with controlled spatial dimensions. The modeled myocyte was replicated in vitro when primary neonate rat ventricular myocytes were cultured on micropatterned substrates. The myocytes remodel to conform to the two dimensional boundary conditions and assume the shape of the printed extracellular matrix island. Mechanical perturbation of the myocyte with an atomic force microscope results in calcium-induced calcium release from intracellular stores and the propagation of a Ca^{2+} wave, as indicated by high speed video microscopy using fluorescent indicators of intracellular Ca^{2+}. Analysis and comparison of the measured wavefront dynamics with those simulated in the computer model reveal that the engineered myocyte behaves as predicted by the model. These results are important because they represent the use of computer modeling, computer-aided design, and physiological experiments to design and validate the performance of engineered cells. The ability to successfully engineer biological cells and tissues for assays or therapeutic implants will require design algorithms and tools for quality and regulatory assurance.

Keywords   Computer-aided design · Cell engineering · Slow Ca^{2+} wave ·
Square myocytes

W. J. Adams · T. Pong · N. A. Geisse · S. P. Sheehy · B. Diop-Frimpong · K. K. Parker (✉)
Disease Biophysics Group, Division of Engineering and Applied Sciences,
Harvard University,
Pierce Hall, 29 Oxford Street, Cambridge, MA 02138, USA
e-mail: kkparker@deas.harvard.edu

1 Introduction

Boundary conditions imposed on a biological cell can potentiate unique behaviors, such as the expression of distinct gene expression profiles [1], compartmentalization of chemical signaling pathways and the self-assembly of unique cytoskeletal architectures [2]. Recent work in soft lithography has resulted in sophisticated cell and tissue culture techniques that allow for control of cell shape [3]. Unfortunately, the production of these assays has been without the integration of computational models of cellular physiology, thus limiting the ability to understand how cell geometry affects quantifiable cellular behavior.

Excitable cells, however, have been the subject of computational studies since Hodgkin and Huxley quantitatively modeled the action potential of the squid giant axon [4]. Cardiac myocytes are no exception, as their complex electrophysiology has been modeled extensively and has played important roles in antiarrhythmic drug discovery and the development of implantable defibrillators [5,6]. Coincidentally, various cardiomyopathies are characterized by changes in ventricular myocyte shape [7], suggesting that within the in vivo tissue microenvironment, maladaptive changes in cell shape may contribute to etiology of disease. The combination of computational modeling of cardiac myocyte physiology with new microfabrication techniques for cell culture presents a powerful opportunity for engineering design of in vitro assays for new therapeutic modalities.

Using numerical simulations of cardiac myocyte electrophysiology, we are able to examine the effects of spatial boundaries and subcellular microenvironments on slow Ca^{2+} wave propagation. Ca^{2+} is an important intracellular messenger, coupling the electrical and mechanical activities that result in cardiac contraction [8]. We have used our model to assess the dynamic properties of slow Ca^{2+} wave propagation in models of geometrically constrained cardiac myocytes. We then used soft lithography to build the modeled myocyte with a freshly harvested ventricular myocyte from a neonate rat. After successful manipulation of the myocyte shape, we conducted experiments to measure the performance of the engineered myocyte against the modeled myocyte. We found that our design algorithm successfully produces cardiac myocytes with electrophysiological properties similar to those predicted from our numerical simulations.

2 Methods

The electrophysiological properties of a cardiac myocyte were numerically simulated. Modeled results were experimentally verified using photolithographic and microcontact printing techniques to engineer an in vitro myocyte to match the geometry of the simulated myocyte. Intracellular Ca^{2+} dynamics were used to assess our ability to translate from myocyte design to fabrication. An overview of our design methodology is depicted in Fig. 1.

2.1 Simulated square myocyte parameters

To simulate Ca^{2+} wave propagation in engineered myocytes, a planar geometric model was developed. The modeled myocyte had a single compartment inside of which Ca^{2+} ions could freely diffuse in two spatial dimensions. Diffusion of Ca^{2+} within the
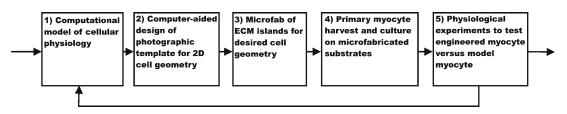
Fig. 1 Schematic of the design algorithm used to build a myocyte with prescribed spatial dimensions and physiological function
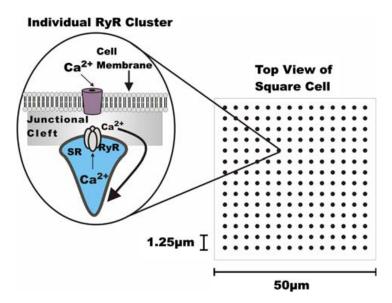

Fig. 2 Diagram of RyR arrangement over the area of a square myocyte membrane. Each node within the myocyte represents one RyR cluster on an SR. (Inset) Exploded diagram of RyR integration between the subcellular SR and subluminal cleft

myocyte could activate calcium-induced, calcium release (CICR) from the sarcoplasmic reticulum, via ryanodine receptors (RyR), which are evenly distributed throughout the myocyte [9]. We modeled the sarcoplasmic reticulum (SR) as a point source injection of Ca^{2+} triggered by a threshold intracellular Ca^{2+} concentration [9]. The SR was spaced at a $1.25\,\mu$m center-to-center pitch over the entire myocyte area. In the whole myocyte action potential model described by Shannon et al. [10], 20,000 individual RyR junctions were modeled over a myocyte area of $15{,}000\,\mu m^2$ (spaced evenly $1.2\,\mu$m apart over the entire myocyte). This density was linearly scaled such that the simulated model accounted for the smaller membrane area in neonatal myocytes that have not yet formed transverse-tubules, invaginations of the surface membrane [11]. Thus, we modeled a density of 1,600 RyR junctions per $2{,}500\,\mu m^2$ myocyte at a similar pitch (Fig. 2). Intracellular buffering, extracellular export, and SR reuptake of Ca^{2+} was modeled as a constant loss of intracellular Ca^{2+}. This constant loss of Ca^{2+} has little effect on wavefront propagation but forces the intracellular Ca^{2+} level to return to a basal state after the wave has terminated. The nucleus of the myocyte and other subcellular structures were not included in the model. Cellular dimensions and parameters are outlined in Table 1.

Table 1 Myocyte geometry and parameters

Parameter	Value	Units
RyR clusters	1,600	nodes
Cell membrane area	2,500	μm^2
Cell side length	50	μm
Mesh size	6,400	nodes
Triangular elements	12,800	triangles
RyR spacing	1.25	μm
$D_{Ca(junction \rightarrow SL)}$	75	$\mu m^2\, s^{-1}$

2.2 Finite element modeling

Simulations were run using MatLab (Mathworks, Natick, MA, USA) on a personal computer with an AMD 3.0 GHz processor and 1,024 MB RAM. The weak formulation of the diffusion equation was solved using a modified program for finite element modeling (FEM) [12]. A standard Galerkin method-based finite element approach was used to model Ca^{2+} diffusion. The diffusion equation in two spatial dimensions was solved for a square myocyte with no convection terms:

$$\frac{\partial u(x,y,t)}{\partial t} = k \left(\frac{\partial^2 u(x,y,t)}{\partial x^2} + \frac{\partial^2 u(x,y,t)}{\partial y^2} \right) \tag{1}$$

with Neumann boundary conditions:

$$\frac{\partial u(x,y,t)}{\partial n} = 0 \text{ on } \Gamma_N, \tag{2}$$

where Γ_N defines the closed boundary of the myocytes with positive length. The Neumann boundary condition confines all released Ca^{2+} within the myocyte, eliminating any diffusive effects through gap junctions and transportation of ions to the extracellular space. Triangular elements were used to create a nodal mesh for the square myocyte. The 80×80 mesh contained 6,400 nodes and 12,800 triangular elements for FEM calculation.

The algorithm generated a stiffness matrix determined by the coordinates of each triangular element. Following the assembly of the stiffness matrix, iterations for the solution matrix were calculated over the time period specified using a time step of $\Delta t = 0.15$ s with incorporation of the Neumann conditions. Previous models of Ca^{2+} metabolism have used a range for the Ca^{2+} diffusion constant that range from 100 [13] to 600 $\mu m^2\, s^{-1}$ [14]. However, in the cytosol the value for diffusion is effectively reduced by a factor of approximately 2.5 due to increased tortuousness, viscosity and the presence of intracellular buffers and obstacles [9]. Our simulations utilized an adjusted Ca^{2+} diffusion constant of 75 $\mu m^2\, s^{-1}$ to account for these obstacles.

To initiate wave propagation, a single RyR was triggered manually, and the model was allowed to run for one full wave cycle. In the analysis, a deterministic rule was adopted for triggering RyR-mediated Ca^{2+} release from the SR. This was chosen over a stochastic model since implementation of stochastic processes significantly increases computational burden. Furthermore, while a stochastic model may be required for higher resolution studies of Ca^{2+} wave genesis, this study focuses exclusively on the mechanics of wave propagation. Thus, a deterministic approach should be sufficient
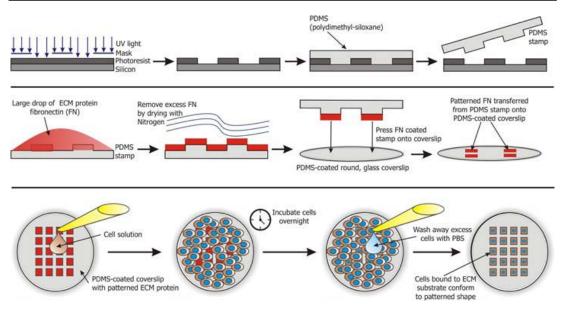
Fig. 3 Microcontact printing (15) and cell culture technique

for studying wave dynamics; each time a SR response is triggered, Ca^{2+} is released into the intracellular space. Diffusion was presumed to dominate the propagation of the slow Ca^{2+} transient.

2.3 Experimental microcontact printing

Cultured myocytes with defined geometries were engineered by microcontact printing the extracellular matrix protein fibronectin (FN, Invitrogen, Carlsbad, CA, USA) onto polydimethyl siloxane (PDMS)-coated glass surfaces [15] (Fig. 3). Using Auto-CAD software (Autodesk, San Rafeal, CA, USA), a 2D photolithographic mask was designed with square islands on the micron length scale to accommodate primary harvest neonate myocytes. This mask was then used to make negative templates of the patterns on silicon wafers coated with SU 8-2 photoresist (MicroChem Corp., Newton, MA, USA) and developed using propylene glycol mono-methyl ether acetate (PGMEA, JTBaker, Phillipsburg, NJ, USA). PDMS (Dow Corning, Midland, MI, USA) was poured over the patterned silicon wafers, cured, and then separated to produce PDMS stamps with the configurations that the myocytes will assume. The surface of each stamp was coated with a solution of FN, dried, and gently brought into contact with sterile PDMS-coated glass coverslips. Then, the stamps were removed and the coverslip was treated with a 1% solution of pluronic F-127 (BASF, Florham Park, NJ, USA) to prevent myocytes from attaching to non FN-coated portions of the coverslip.

2.4 Experimental cell culture

All experiments were conducted in accordance with the guidelines of the Institutional Animal Care and Use Committee of Harvard University. Ventricular tissue was excised from 2-day-old Sprague-Dawley rats (Charles River Laboratories, Wilmington, MA, USA) and enzymatically dissociated with 0.1% solutions of trypsin (USB, Cleveland, OH, USA) and collagenase type 2 (Worthington Biochemical,

Lakewood, NJ, USA) to establish myocyte cultures. Cultured myocytes were maintained in Medium 199 (Invitrogen) supplemented with 10% fetal bovine serum (Invitrogen), 1 M HEPES buffer (Invitrogen), MEM non-essential amino acids (Invitrogen), 3.25 mg/mL glucose, 200 mM L-glutamine, 4 μg/mL vitamin B12, and 50,000 units of penicillin. The serum concentration of the culture medium was reduced to 2% from the second day of culture forward.

2.5 Atomic force microscopy manipulation

To test physiological function of the engineered myocytes, we activated slow Ca^{2+} wave propagation by mechanical perturbation of the myocyte with an atomic force microscope (AFM) during high speed, fluorescence video microscopy. A fluorescent Ca^{2+} indicator, Fluo-4 acetoxymethyl (AM) dye (Invitrogen) in DMSO, was added to cell culture media (6.7 μM) and incubated for 30 min in the dark. After incubation, myocytes were rinsed in Normal Tyrode's (NT, in mM: 137 NaCl, 5.4 KCl, 1.2 $MgCl_2$, 1 $CaCl_2$, 20 HEPES, O_2 saturated, pH = 7.40 measured at 37°C). AFM was performed with an MFP-3D-IO (Asylum Research, Santa Barbara, CA, USA) mounted on an Axiovert 200 MAT optical microscope (Carl Zeiss, Jena, Germany) with a 63X NA 1.4 plan-apochromat objective. Silicon AFM cantilevers (model AC160, Asylum Research) were first calibrated for deflection sensitivity against a glass slide, and then calibrated for their spring constants by measuring cantilever resonance due to thermal fluctuations. Cantilevers were immersed in NT and deflection sensitivity was re-calibrated against a glass slide. The AFM cantilever tip was positioned above the desired part of the myocyte using the coarse adjustment on the AFM stage. A force-deflection curve was taken on the myocyte with the desired impact force used as a stop-trigger. Fluorescence illumination was achieved by an X-cite 120 metal halide arc lamp (Exfo Life Sciences, Mississauga, ON, Canada). Excitation and emission light was separated via a filter cube with the following filtering characteristics (in nm): Excitation Bandpass 450–490, Emission Bandpass 500–575, and dichroic mirror 495. Resultant emission images were collected with a Cascade 512b enhanced-CCD camera (Photometrics Inc., Tuscon, AZ, USA) controlled by an IPLab Spectrum environment (BD Biosciences/Scanalytics, Rockville, MD, USA). Frame rate (28 frames per second) was measured by collection of the frame-readout logical signal from the camera.

2.6 Data analysis

Pixel-wise Ca^{2+} concentration data with respect to time was encoded in a TIF format from both numerical simulation and from experimental image acquisition. The raw concentration data was processed within MatLab using the Image Processing Toolbox. First, the raw data was passed through a 2D Gaussian low pass filter. Second, the time of the maximum discreet derivative of each pixel's Ca^{2+} intensity value with respect to time was computed. The velocity of the wavefront between adjacent points was computed based on the arrival time of the maximum wavefront upstroke ($d[Ca^{2+}]/dt$).
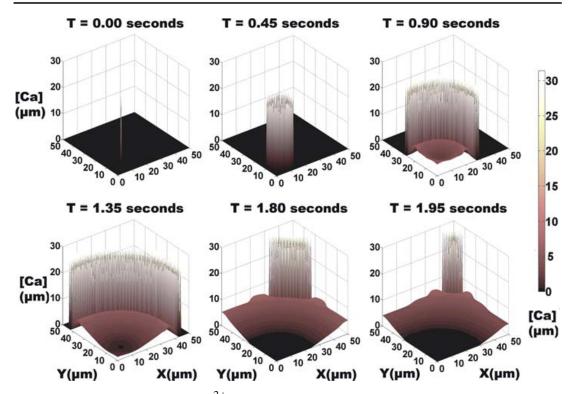
Fig. 4 Simulation results of slow Ca^{2+} wave propagation triggered in the corner of a square cardiac myocyte

3 Results

3.1 Computational modeling of a square cardiac myocyte

We are interested in the pathological consequences of Ca^{2+} slow waves, hence we used our computational model to examine the role of boundary conditions in shaping the wavefront. Simulation of slow Ca^{2+} waves was initiated by the point source injection of intracellular Ca^{2+}, replicating the activation of a single RyR cluster on the SR. Released Ca^{2+} diffuses and triggers CICR at nearby RyR clusters. Time series images of slow Ca^{2+} waves propagating through a modeled $50 \times 50\,\mu$m square myocyte are shown in Fig. 4. The image at $t = 0.00$ s represents the initiation of the Ca^{2+} wave. The sequence of images from $t = 0.45$ to 1.95 s illustrates Ca^{2+} release from individual RyR clusters which sum to the Ca^{2+} wave. The images show that the Ca^{2+} wavefront rises rapidly with progressive recruitment of RyR activity as Ca^{2+} diffuses throughout the myocyte. This is similar to previous observations of Ca^{2+} wave propagation in cardiac myocytes harvested from neonate and adult hearts [16].

3.2 Engineering a square cardiac myocyte

When freshly harvested cardiac myocytes are cultured in tissue culture dishes containing micropatterned surfaces, they will adhere preferentially to the islands of matrix proteins. Post-partum growth of the heart occurs through hypertrophy rather than hyperplasia; thus, when multiple nondividing myocytes occupy a single micropatterned FN island, it is probable that they initially settled on that island (Fig. 5a). Autonomous beating resulted in hypertrophic growth that was directionally guided by geo-
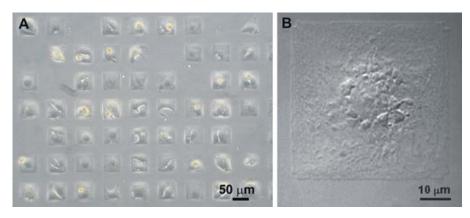
Fig. 5 Phase contrast image of neonatal myocytes cultured on square ECM islands (**a**). **b** shows a differential interference contrast image of a square cardiac myocyte

metric cues in the micropatterned extracellular matrix. Thus, the initially pleomorphic myocytes spread and assumed the shape of the island (Fig. 5b).

3.3 Experimental observation of slow Ca^{2+} waves

In order to test the behavior of our engineered myocytes against the simulated myocytes, we loaded the square myocytes with a fluorescent Ca^{2+} indicator and initiated slow Ca^{2+} wave propagation by AFM indentation. A $1\,\mu N$ force was quickly applied with the AFM cantilever tip orthogonal to the plane of the substrate after experimental determination of the threshold force required to induce Ca^{2+} release. Upon indentation, the local Ca^{2+} release was sufficient to induce the propagation of a Ca^{2+} wave throughout the square myocyte by means of CICR (Fig. 6). The total time taken to traverse the myocyte was 2.2 s corresponding to an average wave velocity of $36.6\,\mu m\,s^{-1}$. Within our simulation, the time taken to traverse the myocyte was 2.1 s resulting in an average wave velocity of $45.4\,\mu m\,s^{-1}$. Both wave velocities agree well with previously reported velocities in the range of 40–$180\,\mu m\,s^{-1}$ [16].

Isochrone plots of slow Ca^{2+} waves in engineered and modeled square myocytes are compared in Fig. 7. The wave can be seen to propagate from the corner (where the force was applied) across the middle of the myocyte to the opposite corner. The wavefront velocity demonstrated a marked increase when propagating into the opposite corner while the wavefront is at minimum velocity in the center of the myocyte.

The effects of geometric boundaries in the square myocyte are also apparent in the isochrone plots as the concavity of the wavefront flipped orientation during propagation across the myocyte. A flip in wavefront concavity implies a difference in wavefront velocity between the center of the myocyte and the perimeter. In the experimental data, this change of concavity occurred earlier in the wave's propagation than in the simulation. This divergence between experiment and simulation may be a result of the differences between our two dimensional model and the 3D structure of in vitro myocytes. Cardiac myocytes that have been engineered through microcontact printing consistently possess a greater height in the perinuclear region. On the contrary, the simulation assumed a constant height everywhere under the myocyte membrane. Additionally, the simulated myocyte lacks subcellular structure, such as a nucleus and mitochondria, which may pose as an impediment to Ca^{2+} diffusion. These limiting assumptions of the model can explain the differences in wavefront dynamics
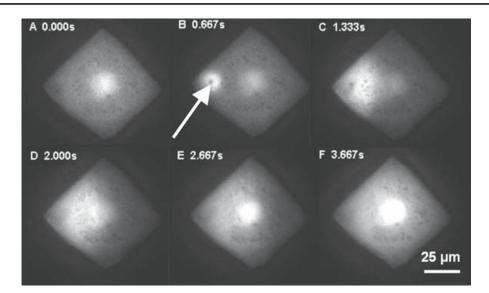
Fig. 6 AFM-induced slow Ca^{2+} wave propagation. *White arrow* indicates the location of indentation. Intracellular Ca^{2+} concentration was visualized with fluorescent Ca^{2+} indicator dye. The bright circular spot in the middle of the myocyte is the nucleus
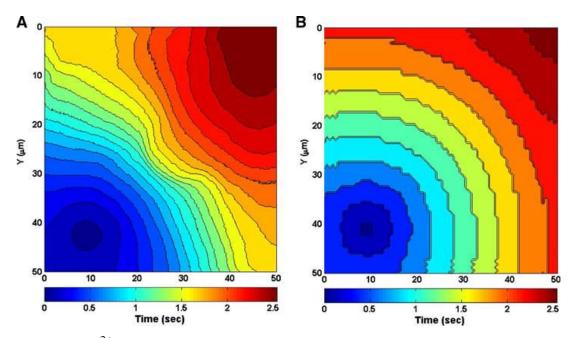

Fig. 7 Slow Ca^{2+} wave isochrones during propagation in experiment (**a**) and simulation (**b**)

4 Discussion

This paper describes an algorithm for the engineering of cardiac myocytes in vitro with desired shape and Ca^{2+} processing. Such an assay would offer a powerful means for exploring the role of myocyte shape in cardiomyopathies and the concurrent changes in Ca^{2+} metabolism. While the microfabrication of cell tissue culture environments has been reported for nearly a decade, the use of computational models of cellular physiology has traditionally not been applied in cellular engineering. Detailed models of cardiac myocyte physiology, such as that by Shannon et al., incorporate the

molecular components of signaling pathways that potentiate myocyte function. This is important for identifying and validating therapeutic drug targets.

Engineered cells also reveal deficiencies in our computational models. For example, our experimental results suggest that the nuclear Ca^{2+} dynamics alter the wavefront velocity and contribute to changes in the shape of the wavefront. Previous work by Genka et al. [17] suggests that the delayed nuclear Ca^{2+} transient is dependant upon Ca^{2+} diffusion across the nuclear membranes. The slowing of the Ca^{2+} wave, and localized change in wavefront shape as indicated by the isochrones in Fig. 7, suggest that the nucleus is capable of altering the wavefront dynamics. Further studies will reveal if this is a functional or dysfunctional influence, with the answer most likely depending on the shape of the myocyte, the architecture of the transverse-tubule system, and whether or not the myocyte is binucleated as are most adult ventricular myocytes. Additionally, restricted diffusive space at boundaries forces a faster wavefront velocity parallel to the boundaries. These intracellular velocity gradients may potentiate spiral Ca^{2+} waves as reported by Genka et al. that could theoretically contribute to cardiac arrhythmogenesis.

5 Conclusions

Our numerical model serves as a mechanism for designing cardiac myocytes with specific physiological characteristics. Custom designed myocytes can be engineered through microfabrication and microcontact printing techniques where spatial boundaries are imposed upon cardiac myocytes by printing extracellular matrix proteins to which myocytes preferentially bind. Numerical simulation offers insight in design while subsequent analysis of in vitro myocytes provides closed-loop feedback for optimization of the design process.

References

1. Chen, C.S., Mrksich, M., Huang, S., Whitesides, G.M., Ingber, D.E.: Geometric control of cell life and death. Science **276**, 1425–1428 (1997).
2. Parker, K.K., Brock, A.L., Brangwynne, C., Mannix, R.J., Wang, N., Ostuni, E., Geisse, N.A., Adams, J.C., Whitesides, G.M., Ingber, D.E.: Directional control of lamellipodia extension by constraining cell shape and orienting cell tractional forces. FASEB J. **16**(10), 1195–1204 (2002).
3. Dike, L.E., Chen, C.S., Mrksich, M., Tien, J., Whitesides, G.M., Ingber, D.E.: Geometric control of switching between growth, apoptosis, and differentiation during angiogenesis using micropatterned substrates. In Vitro Cell. Dev. Biol. Anim. **35**, 441–448 (1999).
4. Hodgkin, A.L., Huxley, A.F., Katz, B.: Measurement of current-voltage relations in the membrane of the giant axon of Loligo. J. Physiol. **116**, 424–448 (1952).
5. Kleber, A.G., Rudy, Y.: Basic mechanisms of cardiac impulse propagation and associated arrhythmias. Physiol. Rev. **84**(2), 431–488 (2004).
6. Priori, S.G., Barhanin, J., Hauer, R.N., Haverkamp, W., Jongsma, H.J., Kleber, A.G., McKenna, W.J., Roden, D.M., Rudy, Y., Schwartz, K., Schwartz, P.J., Towbin, J.A., Wilde, A.M.: Genetic and molecular basis of cardiac arrhythmias: impact on clinical management parts I and II. Circulation **99**(4), 518–528 (1999).

7. Gerdes, A.M., Capasso, J.M.: Structural remodeling and mechanical dysfunction of cardiac myocytes in heart failure. J. Mol. Cell. Cardiol. **27**(3), 849–856 (1995).
8. Bers, D.: Cardiac exciation-contraction coupling. Nature **415**, 198–205 (2002).
9. Smith, G.D., Keizer, J.E., Stern, M.D., Lederer, W.J., Cheng, H.: A simple numerical model of calcium spark formation and detection in cardiac myocytes. Biophys. J. **75**, 15–32 (1998).
10. Shannon, T.R., Wang, F., Puglisi, J., Weber, C., Bers, D.M.: A mathematical treatment of integrated Ca dynamics within the ventricular myocyte. Biophys. J. **87**, 3351–3371 (2004).
11. Brette, F., Orchard, C.: T-tubule function in mammalian cardiac myocytes. Circ. Res. **92**, 1182–1192 (2003).
12. Alberty, J., Carstensen, C., Funken, S.: Remarks around 50 lines of Matlab: short finite element implementation. Num. Algorithms. **20**, 117–137 (1999).
13. Langer, G.A., Peskoff, A.: Calcium concentration and movement in the diadic cleft space of the cardiac ventricular cell. Biophys. J. **70**, 1169–1182 (1996).
14. Pratusevich, V.R., Balke, C.W.: Factors shaping the confocal image of the calcium spark in cardiac muscle cells. Biophys. J. **71**, 2942–2957 (1996).
15. Tan, J., Liu, W., Nelson, C., Raghavan, S., Chen, C.: A simple approach to micropattern cells on common culture substrates by tuning substrate wettability. Tissue Eng. **10**, 865–872 (2004).
16. Baader, A.P., Buchler, L., Bircher-Lehmann, L., Kleber, A.: Real time, confocal imaging of Ca(2+) waves in arterially perfused rat hearts. Cardiovasc. Res. **53**, 105–115 (2002).
17. Genka, C., Ishida, H., Ichimori, K., Hirota, Y., Tanaami, T., Nakazawa, H.: Visualization of biphasic Ca^{2+} diffusion from cytosol to nucleus in contracting adult rat cardiac myocytes with an ultra-fast confocal imaging system. Cell Calcium **25**, 199–208 (1999).